Journal of Alloys and Compounds 504 (2010) 303–309

Contents lists available at ScienceDirect

Journal of Alloys and Compounds

journal homepage: www.elsevier.com/locate/jallcom

Room temperature Young's modulus, shear modulus, and Poisson's ratio of $Ce_{0.9}Fe_{3.5}Co_{0.5}Sb_{12}$ and $Co_{0.95}Pd_{0.05}Te_{0.05}Sb_3$ skutterudite materials

Robert D. Schmidt[a], Jennifer E. Ni[a], Eldon D. Case[a,*], Jeffery S. Sakamoto[a], Daniel C. Kleinow[a], Bradley L. Wing[a], Ryan C. Stewart[a], Edward J. Timm[b]

[a] Chemical Engineering and Materials Science Department, Michigan State University, East Lansing, MI 48824, USA
[b] Mechanical Engineering Department, Michigan State University, East Lansing, MI 48824, USA

ARTICLE INFO

Article history:
Received 7 November 2009
Received in revised form 31 May 2010
Accepted 2 June 2010
Available online 11 June 2010

Keywords:
Thermoelectric materials
Elasticity
Ultrasonics
Microstructure
Nanoindentation

ABSTRACT

Room temperature Young's modulus, shear modulus and Poisson's ratio were measured by Resonant Ultrasound Spectroscopy (RUS) for a total of 29 skutterudite specimens cut from four hot pressed billets: (i) two p-type ($Ce_{0.9}Fe_{3.5}Co_{0.5}Sb_{12}$) billets, (ii) one n-type ($Co_{0.95}Pd_{0.05}Te_{0.05}Sb_3$) billet with 0.1 atomic% Ce addition and (iii) one n-type billet without Ce addition. Within a given hot pressed billet, the elastic moduli were very uniform from specimen to specimen. Also, Ce-doping of the n-type specimens did not result in a significant shift in the elastic modulus. For n-type specimens with 98% relative density, the mean Young's modulus, shear modulus and Poisson's ratio were 140.6 ± 0.2 GPa, 57.34 ± 0.05 and 0.226 ± 0.001 GPa, respectively. For the p-type specimens of similar relative density, the mean Young's and shear moduli were approximately 7% lower than the n-type, while there was no significant difference between the mean Poisson's ratio values of the n-type and p-type 98% dense specimens. The measured elastic moduli agreed relatively well with the literature values for other Sb-based skutterudite compositions. In addition, nanoindentation measurements on three mutually orthogonal specimen faces showed no appreciable anisotropy in Young's modulus.

1. Introduction

Efforts to reduce energy consumption and use of fossil fuels have created the impetus to develop new energy efficient technologies [1]. Thermoelectric technology is a solid state technology in which heat flowing through heavily-doped semiconductor elements is converted into a direct current electrical flux [2,3], thus potentially improving the energy efficiency of industrial processes and internal combustion engines used in transportation [2,4–8]. Whether the heat is captured from a radiant heat source, exhaust gas or a solid heat exchanger, significant thermomechanical stresses can be generated when the thermoelectric elements are thermally cycled.

The elastic moduli of thermoelectric materials are important mechanical properties to characterize since the elastic moduli are required for either numerical or analytical analysis of stress strain behavior. For example, for finite element analysis (FEA), Young's modulus and Poisson's ratio are typically used to construct the required stiffness matrix [9,10]. In addition, the elastic moduli are sensitive to the dimensions and volumetric number density of microcracks in a specimen [11–13] or specimen porosity [14,15], thus for a given material the elasticity is a gauge of the defect state of a specimen. Therefore mechanical property characterization is needed as a guide to thermoelectric generator design.

Currently, there are several promising materials systems under consideration for waste heat recovery [2,4]; however this study is focused on skutterudite-based materials. Bulk skutterudite-based materials typically have a high thermoelectric conversion efficiency (or ZT) in the 200–700 °C temperature range. A wide operating range is a key aspect when considering the practicality of thermoelectric waste heat recovery since efficiency increases as the thermal gradient increases.

In this study, we measured Young's modulus, shear modulus and Poisson's ratio of the antimony-based skutterudite compositions $Ce_{0.9}Fe_{3.5}Co_{0.5}Sb_{12}$ (p-type) and $Co_{0.95}Pd_{0.05}Te_{0.05}Sb_3$ (n-type) skutterudite using Resonant Ultrasound Spectroscopy (RUS). For the n-type skutterudite composition, the elasticity was measured for specimens both with and without 0.1 atomic% cerium doping. Since in general as-cast thermoelectric specimens tend to have grain sizes of several hundred microns or larger and such large grain sizes lead to poor mechanical integrity [16–19], all specimens included in this study were cast, powder processed [20,21] and then hot pressed. In addition to the RUS measurements, Young's modulus was measured for the Ce-doped and undoped n-type specimens

* Corresponding author.
E-mail address: casee@egr.msu.edu (E.D. Case).

0925-8388/$ – see front matter © 2010 Elsevier B.V. All rights reserved.
doi:10.1016/j.jallcom.2010.06.003

using nanoindentation on three mutually perpendicular faces of the rectangular parallelepiped specimens.

2. Experimental procedure

2.1. Specimen preparation and microstructural characterization

For both the n-type and p-type skutterudite specimens included in this study, approximately 100 g of the constituent materials was melted together in a sealed glassy carbon crucible to cast an ingot. In order to obtain specimens with a smaller grain size than the as-cast state, the cast ingots were then powder processed.

Each powder processing step was performed in an argon atmosphere inside a glove box (Omni-Lab double glove box) equipped with an oxygen sensor and a moisture sensor (Vacuum Atmospheres Company, Hawthorne, CA). Inside the glove box, the sealed glassy carbon crucible was broken to remove the cast ingot. The ingot was then crushed by hand with a steel mallet to obtain particle sizes approximately 1 mm or less in diameter. The resulting particles were crushed and ground for 5 min using a mechanical mortar and pestle (Retsch RM200, Retsch GmbH, Haan, Germany). The ground powder that did not pass through a 75 μm sieve was reground. The regrinding process continued until all powders passed through the 75 μm sieve, which typically required a total of 3–5 regrinding steps per 100 g ingot.

The crushed, ground, sieved and reground (CGSR) powders were then used in the CGSR state or either: (1) wet milled only or (2) first dry milled and then wet milled (Table 1). All dry and wet milling procedures were performed in a planetary ball mill (Retsch PM100) using a 500-mL stainless steel milling jar. After each dry and wet milling run, the powders that adhered to the walls of the milling jar were removed by scraping with a metal spatula. Powder batches of approximately 23–25 g of CGSR powder were dry milled for 3 h at 150 rpm in the planetary ball mill using approximately 230 g of 10 mm diameter spherical 440C stainless steel media or 20 mm diameter spherical 420 stainless steel media. Wet milling was performed with 21–24 g of dry milled powders that were milled with 25 mL of hexane for 6 h at mill speeds of 110 rpm using 170 g of 3 or 6 mm diameter 440C stainless steel spheres and 230 g of 20 mm 420 stainless steel spheres.

The CGSR and wet milled powders were hot pressed at 620–650 °C at pressures of about 75 MPa for 2 h. The powder processing and hot pressing parameters for the specimens included are summarized in Table 1.

Specimens for subsequent mechanical property and microstructural analysis were cut from hot pressed billets using a K.O. Lee Surface Grinder (5361 SHS, K.O. Lee Co, Aberdeen, South Dakota). For the Resonant Ultrasound Spectroscopy analysis, rectangular parallelepiped specimens nominally 10 mm × 7 mm × 2 mm or 10 mm × 7 mm × 5 mm were cut from the hot pressed billets. Each of the specimen dimensions was calculated from the mean of at least five measurements made at different locations along the specimen using electronic calipers with an accuracy of ±0.001 mm (Mitutoyo CD-6"CSX, Kanagawa, Japan). The specimen mass was measured to ±0.0003 g accuracy using an electronic balance (Adventurer AR2140, Ohaus Corp., Pine Brook, NJ). Specimen mass densities were calculated from the mean specimen dimensions and specimen mass. Specimens used for microstructural analysis were mounted in thermoplastic and polished on an automatic polishing machine (Leco Vari/Pol VP-50, Leco Corporation, St. Joseph, MI) with successively smaller diamond grit paste from 90 to 1 μm.

For microstructural characterization, specimen surfaces that were either (i) polished or (ii) fractured were examined with a scanning electron microscope (JEOL 6400, JEOL Ltd., Japan) using a working distance of 15 mm and an accelerating voltage of 15 kV. The specimen surfaces were sufficiently electrically conductive that no conductive coatings were applied prior to SEM examination. The as-polished specimen surfaces were examined to determine the size and shape of the surface pores and to determine whether or not surface-breaking cracks were present. Using SEM micrographs of fracture surfaces, the mean grain size was determined using the linear intercept technique and a stereographic projection factor of 1.5.

Samples of the powders used to hot press cerium-doped SKD-Wet1 and the undoped SKD-Wet2 were examined by X-ray diffraction (XRD) using a Rigaku Rotaflex 200B diffractometer, Cu Kα X-ray radiation and a curved crystal graphite monochromator (Rigaku Corp., Tokyo, Japan) with a NaI Scintillation Detector and a graphite filter. An anode voltage of 45 kV and current of 100 mA were used. The powder specimen was placed in a silica sample holder designed for low background and vertical placement. The powder specimen was tightly packed to prevent powder loss during collection of the XRD pattern. No background correction was applied to raw data. Measurements were taken for 2θ angles of 10–90° with a step size of 0.05° and a speed of 1° 2θ/min.

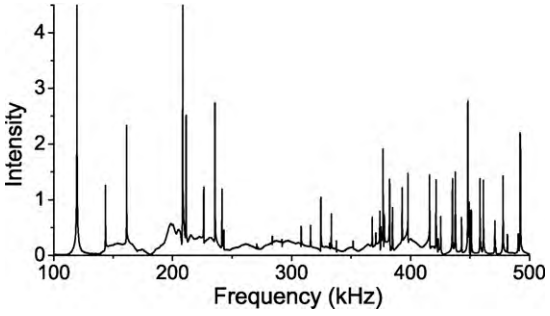

Fig. 1. A plot of the mechanical resonant frequency spectrum for specimen n-Ce-Wet1-A, which is typical of the resonant frequency spectra of each of the specimens included in this study.

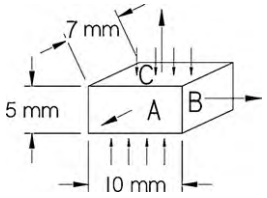

Fig. 2. Schematic of the three mutually orthogonal specimen faces of the Ce-doped and undoped skutterudite specimens that were nanoindented in order to determine if significant elasticity anisotropy was present in the specimens. Face C (7 mm × 10 mm) was normal to the pressing direction, while face A (5 mm × 10 mm) and face B (5 mm × 7 mm) were orthogonal to the pressing direction. The pressing direction is indicated by vertical arrows in the figure.

2.2. Resonant Ultrasound Spectroscopy

Young's modulus, E, shear modulus, G, and Poisson's ratio, ν, were measured for the $Ce_{0.9}Fe_{3.5}Co_{0.5}Sb_{12}$ and $Co_{0.95}Pd_{0.05}Te_{0.05}Sb_3$ skutterudite materials using commercial Resonant Ultrasound Spectroscopy (RUS) equipment (Quasar RUSpec, Quasar International, Albuquerque, NM) [22]. The specimens were placed on a tripod arrangement of transducers with one driver transducer and two pick up transducers. The mechanical resonance frequencies of each specimen were determined as the sinusoidal driving frequency was swept through a range of 20–700 kHz. Based on the specimen dimensions, mass, and resonant frequency spectrum (Fig. 1), Young's modulus, shear modulus and Poisson's ratio were calculated using the software provided with the RUS apparatus (Quasar Galaxy RI2000 and RPModel software, Quasar International). Between 14 and 24 resonance frequencies were used to calculate each of the modulus values. Additional details of the RUS experimental procedure are given elsewhere [23,24].

2.3. Nanoindentation

For cerium-doped SKD-Wet1 specimen and of undoped SKD-Wet2, the extent of elastic anisotropy was investigated by nanoindenting each of the two specimens on three mutually orthogonal specimen faces, labeled faces A, B, and C (Fig. 2). The outward normal directions to faces A and B were perpendicular to the hot pressing direction while the outward normal to face C was parallel to the hot pressing direction.

The nanoindented surface of a 6061 aluminum standard specimen and all nanoindented surfaces of the two skutterudite specimens were polished with diamond paste prior to nanoindentation to a minimum grit size of 1 μm. Using a Nanoindenter XP with CSM/LFM (MTS, Oak Ridge, TN) a minimum of 20 nanoindentations per specimen face were placed in areas free of scratches or other surface defects. For all nanoindentations, a Berkovitch indenter tip was employed with a nanoindentation depth of 2000 nm. Sixteen nanoindentations per specimen face were placed in a 4 × 4 array with a 50 μm spacing between each nanoindentation. Also minimum of four additional nanoindentations were placed in manually selected locations near 4 × 4 nanoindentation array on the skutterudite specimen

Table 1
Powder processing parameters for the n-type and p-type hot pressed billets included in this study.

Billet label	Composition	Type	Milled or CGSR	Max. temp. (°C)	Time at temp. (min)	Pressure (MPa)
n-Ce-Wet1	$Co_{0.95}Pd_{0.05}Te_{0.05}Sb_3$ doped with 0.1 atomic% cerium	n-Type	Dry then Wet	650	120	74.4
n-Wet2	$Co_{0.95}Pd_{0.05}Te_{0.05}Sb_3$	n-Type	Dry then Wet	650	120	74.4
p-CGSR	$Ce_{0.9}Fe_{3.5}Co_{0.5}Sb_{12}$	p-Type	CGSR	620	120	74.4
p-Wet3	$Ce_{0.9}Fe_{3.5}Co_{0.5}Sb_{12}$	p-Type	Wet milled only	640	120	74.9

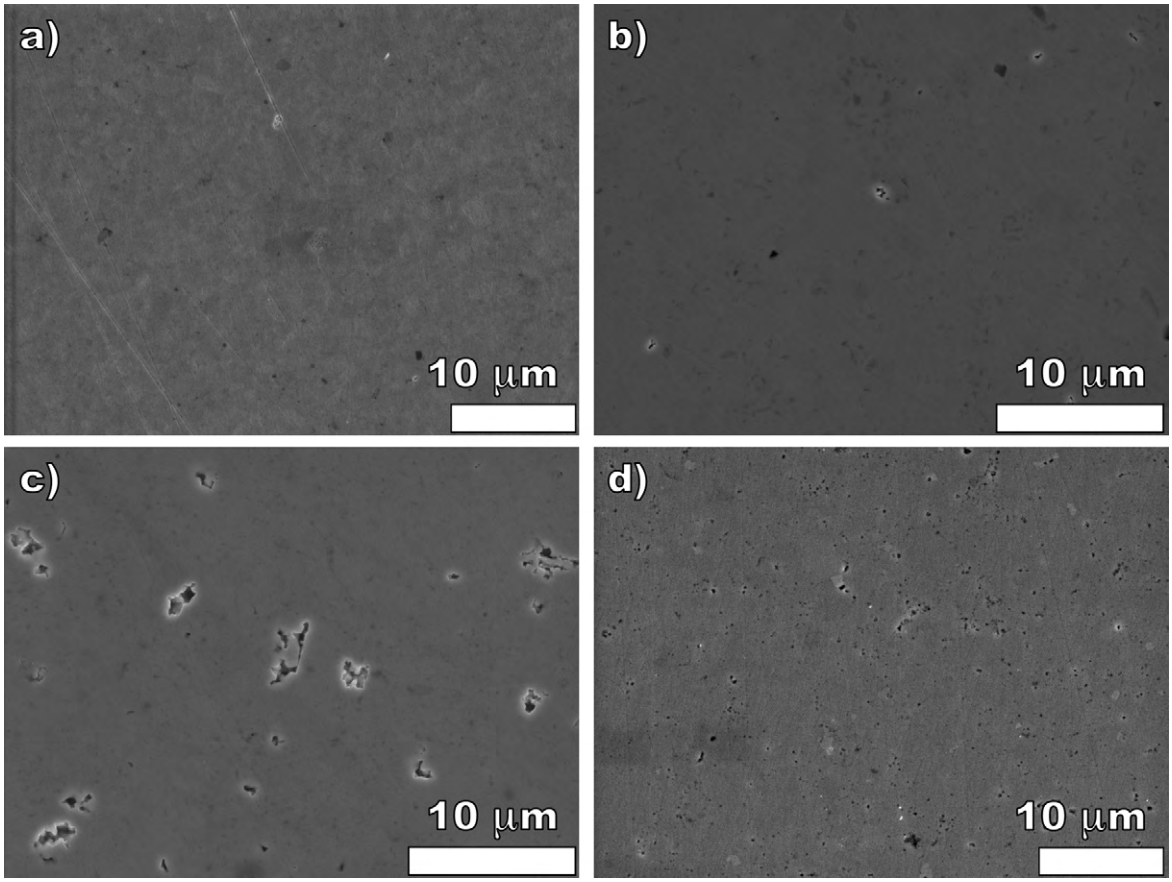

Fig. 3. SEM micrographs of the as-polished surfaces of specimens cut from each of the four hot pressed skutterudite billets included in this study: (a) n-Ce-Wet1, (b) p-CGSR, (c) p-Wet3 and (d) n-Wet2. Note that each specimen surface is free of cracks and large pores.

faces. A similar array of 16 nanoindentations was placed on the surface of the 6061 aluminum standard specimen.

3. Results and discussion

3.1. Microstructural and XRD analysis

An SEM examination was done on polished surfaces (Fig. 3a–d) as well as the fractured surfaces of the polished specimens (Fig. 4a–d) for selected specimens cut from each of the four hot pressed billets included in this study. No surface-breaking cracks were observed via SEM in the as-polished surfaces of the $Ce_{0.9}Fe_{3.5}Co_{0.5}Sb_{12}$ and $Co_{0.95}Pd_{0.05}Te_{0.05}Sb_3$ specimens (Fig. 3a–d). For billets n-Ce-Wet1 and p-CGSR, the surface pores were isolated, quasi-spherical and were typically 1 μm or less across (Fig. 3a and b). For billet p-Wet3, the pores were polygonal, about 1–3 μm across and frequently appeared in clusters of from two to four pores (Fig. 3c). For billet n-Wet2, numerous quasi-spherical or lenticular surface pores about 1 μm across or smaller were observed, often in clusters of a few pores or in linear arrays of several pores (Fig. 3d). The fractured specimens (Fig. 4a–d) showed relatively equiaxed grain shape with mean grain sizes ranging from approximately 0.6–1.5 μm (Table 2). For billet p-CGSR, the mean grain size of the matrix is approximately 0.6 μm (Fig. 4b); however numerous larger grains 5–50 μm in diameter were uniformly distributed throughout the matrix. An areal number density of about 15 per 1000 μm^2 of the larger grains (5–50 μm across) were observed in SEM micrographs of the p-CGSR specimen, with the large grain fraction accounting for about 11% of the fracture surface. SEM micrographs of fracture surfaces of all specimens included in this study showed that pores were present at the grain boundaries and triple points. No entrapped porosity was observed in any of the specimens.

The XRD diffraction patterns were compared to the powder diffraction file for $CoSb_3$, 83-0055 [25], for both the Ce-doped and the undoped specimens (Fig. 5). However the Ce-doped powders show three additional broad peaks at 2θ values of 31.998°, 33.747° and 34.703°, corresponding to d-spacings of 2.7947, 2.6538 and 2.5828 Å, likely indicate the presence of a minority of $CoSb_2$ mixed with the majority material, as the peaks correspond with the three most intense peaks in XRD pattern for $CoSb_2$, 29-0126 [26].

In general, X-ray line broadening can arise from either crystallite size effects or strain effects although the magnitude of strain-induced broadening is relatively modest [27]. The three broad peaks that appear in the XRD pattern for the Ce-doped skutterudite are consistent with particle size broadening effects for crystallites that are roughly 0.1 μm or smaller in size [27], thus the Ce-doped may be enhancing the precipitation of submicron $CoSb_2$ particles in the matrix, but further research should be done to determine the detailed effects of the Ce-doping in the skutterudite materials included in this study.

Table 2
Mean grain size determined by the linear intercept technique on SEM micrographs of fracture surfaces using a stereographic projection factor of 1.5.

Billet label	Type	Mean grain size
n-Ce-Wet1	n-Type	1.0 μm
n-Wet2	n-Type	1.5 μm
p-CGSR	p-Type	0.6 μm*
p-Wet3	p-Type	1.2 μm

* The mean grain size for p-CGSR is for the matrix. The matrix contains numerous grains of 5–50 μm diameter.

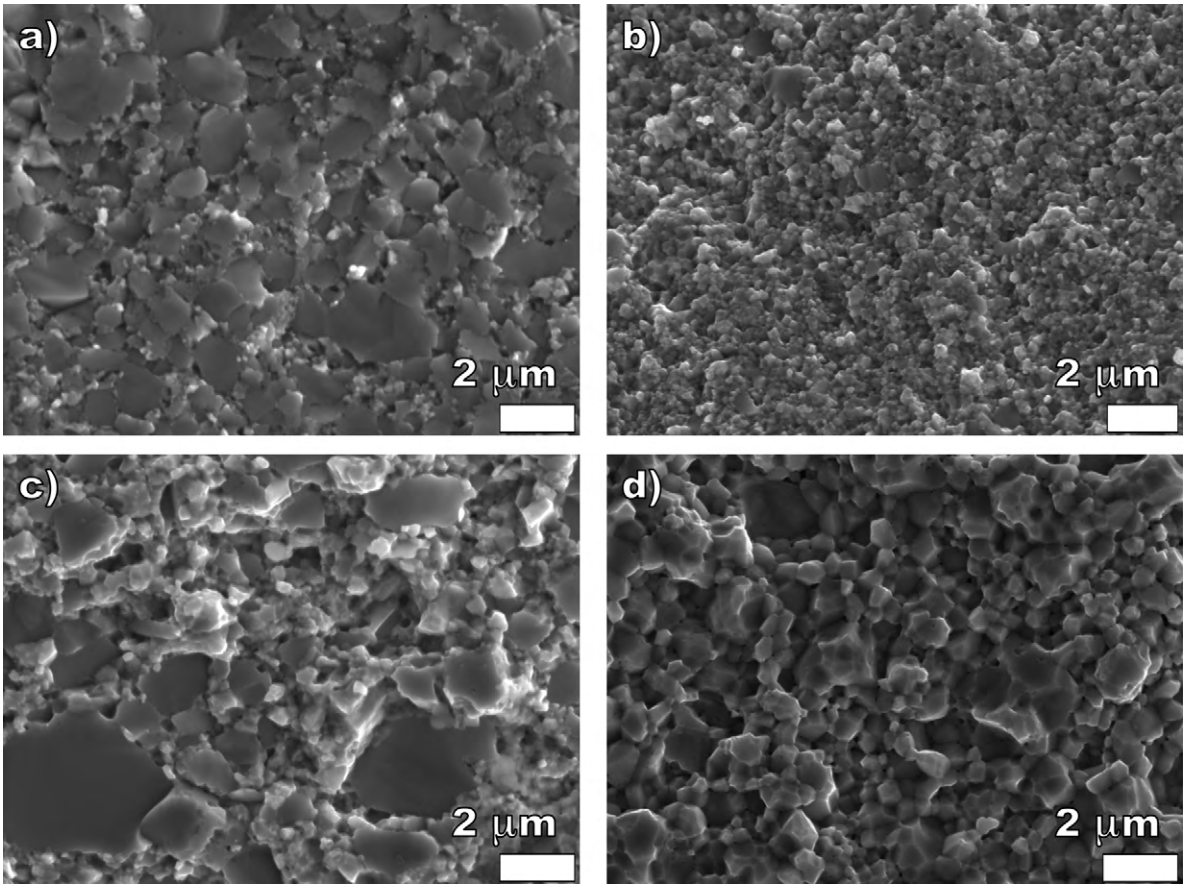

Fig. 4. SEM micrographs of the fracture surface of specimens cut from each of the four hot pressed skutterudite billets included in this study: (a) n-Ce-Wet1, (b) p-CGSR, (c) p-Wet3 and (d) n-Wet2. In each case, the grains are relatively equiaxed with pores present at the grain boundaries and/or triple points. No entrapped porosity was observed.

3.2. Elastic modulus measurements via RUS

In this study, the room temperature elastic moduli (Young's modulus, shear modulus and Poisson's ratio) were measured for a total of 29 specimens that were cut from four billets, two billets each of n-type and p-type skutterudite materials (Table 3). For the six specimens cut from n-Ce-Wet1, the Ce-doped n-type hot pressed billet ($Co_{0.95}Pd_{0.05}Te_{0.05}Sb_3$, with a 0.1 atomic% Ce addition), the mean and standard deviation of the room temperature RUS values of Young's modulus, E, was 140.6 ± 0.2 GPa and mean shear modulus, G, was 57.34 ± 0.05 GPa (Table 3). For the eight specimens cut from n-Wet2, the n-type billet without Ce-doping, the mean and standard deviation of the E and G values were 137.8 ± 1.2 and 56.01 ± 0.26 GPa, respectively (Table 3).

The elastic moduli of the hot pressed n-type billets were relatively uniform within each billet. For example, the coefficient of variation (standard deviation/mean) was only 0.14 and 0.08% for the E and G values, respectively, for the specimens cut from the Ce-doped n-type billet (Table 3). For the n-type billet without Ce-doping, the coefficients of variation were 0.88 and 0.46% for the E and G data, respectively (Table 3). In addition, for the n-type billets with and without Ce-doping, the E and G values agreed to within about 2.0 and 2.3%, respectively, which indicates that the 0.1 atomic% cerium doping may result in a slight increase in the elastic moduli of the n-type specimens (Table 3). However, an alternative explanation is that the higher mass density of the Ce-doped specimen (Table 3) may account for part or all of the observed difference in E and G, since the elastic moduli of solids decrease with increasing volume fraction porosity [28].

For the specimens cut from the two p-type billets (Table 3), Young's modulus and shear modulus was at least 5% lower than the moduli of the n-type billets. For the n-type and p-type billets, there is a considerable difference in the chemical composition (Table 1) which might account for the differing moduli. However, as was the case with the n-type skutterudite, within a given p-type billet, Young's modulus and shear modulus values were again uniform (Table 3). Also, the differences between the average moduli between the two p-type billets may be a function of the volume fraction porosity of the billets. As was the case for the n-type billets; the p-type billet with the higher mass density had the higher moduli. However, to determine the extent to which the differences between the elastic moduli of the n-type and p-type billets are

Table 3
Resonant Ultrasound Spectroscopy measurements of the mean and standard deviation of Young's modulus, E, shear modulus, G, and Poisson's ratio, ν, for multiple specimens cut from the indicated hot pressed billets.

Billet label	Number of specimens	Resonance peaks fitted	Type	Density (g/cm^3)	Relative density	E (GPa)	G (GPa)	ν
n-Ce-Wet1	6	14–24	n-Type	7.59	0.977	140.6 ± 0.2	57.34 ± 0.05	0.226 ± 0.001
n-Wet2	8	14–22	n-Type	7.45	0.960	137.8 ± 1.2	56.01 ± 0.26	0.231 ± 0.006
p-CGSR	7	15–23	p-Type	7.73	0.975	131.2 ± 0.6	53.58 ± 0.54	0.230 ± 0.008
p-Wet3	8	15–24	p-Type	7.57	0.956	126.8 ± 0.4	51.04 ± 0.30	0.242 ± 0.011

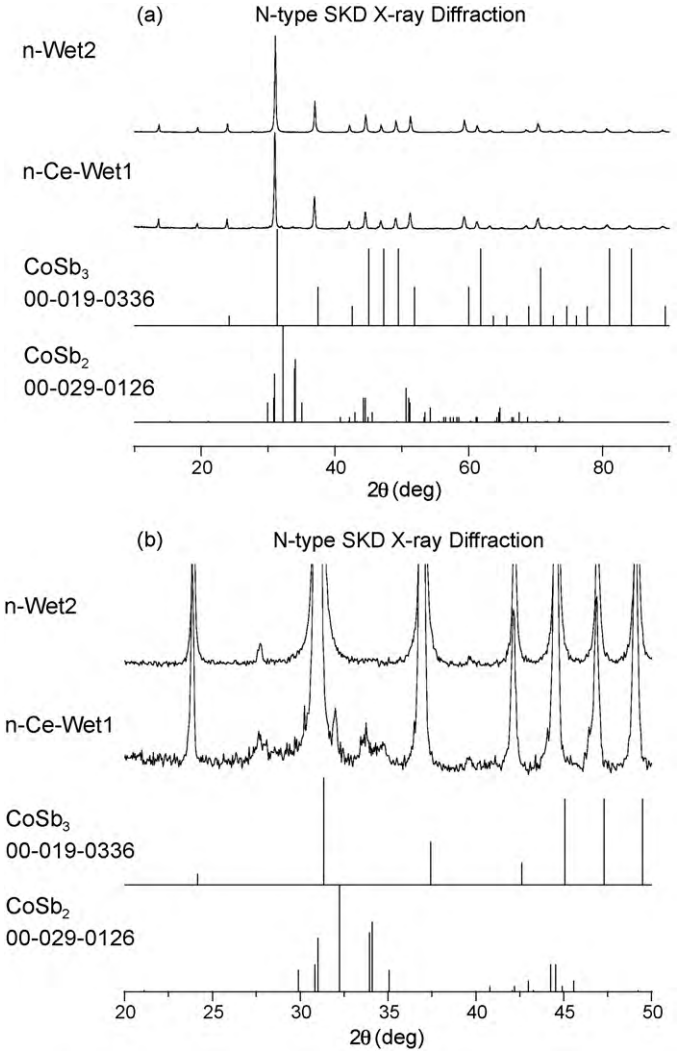

Fig. 5. X-ray diffraction of two n-type specimens, the undoped n-Wet2 and the Ce-doped n-Ce-Wet1. (a) Nearly all peaks in both X-ray patterns correspond to the unfilled skutterudite $CoSb_3$ [25], as seen through the entire range from 2θ angles of 10° through 90°. (b) Details of the 2θ range between 30° and 36° for n-Ce-Wet1 with three broad peaks that correspond to the intense peaks in the $CoSb_2$ pattern [26].

attributable to mass density would require a study of the elastic modulus versus mass density for a number of mass density values.

No literature data exists for elastic moduli for the n-type and p-type skutterudite compositions included in this study. However, there are literature values for elastic moduli of n-type and p-type Sb-based skutterudite materials with compositions roughly similar to that of the specimens included in this study [29,30] (Table 4). Ravi et al. [29] used the impulse excitation method to determine Young's modulus, E, and shear modulus, G, and Poisson's ratio, ν, for n-type doped $CoSb_3$, and p-type $CeFe_{3-x}Ru_xSb_4$ (note that the chemical formula given by Ravi, $CeFe_{3-x}Ru_xSb_4$, does not correspond to the usual stoichiometry for a skutterudite material). Also, Recknagel et al. [30] used ultrasonic and nanoindentation measurements to determine E of $CoSb_3$ (n-type) and $LaFe_4Sb_{12}$ (p-type) skutterudite materials. Thus, for both n-type and p-type skutterudites with chemical composition somewhat similar to those in this study, the E and G values measured by Ravi et al. [29] as well as the E values obtained by Recknagel et al. [30] compare well to the corresponding values in this study (Table 4).

Based on this study's RUS measurements, the mean values of Poisson's ratio were 0.226 and 0.231 for the n-type billets and 0.230 and 0.243 for the p-type billets (Table 3). In comparison, Poisson's ratio values reported by Ravi et al. [29] ranged from 0.14 to 0.25 for the n-type doped $CoSb_3$ and from 0.22 to 0.29 for the p-type $CeFe_{3-x}Ru_xSb_4$ (Table 4). Especially for the n-type $CoSb_3$, the range of Poisson's ratio reported by Ravi et al. [29] is quite wide compared to the range of Poisson's ratio values obtained in this study for the n-type and p-type skutterudites.

3.3. Elastic modulus measurements by nanoindentation

Young's modulus values obtained via nanoindentation (Table 5) on the three mutually orthogonal faces of both the Ce-doped and the undoped n-type skutterudite specimens indicated that there was no significant elastic anisotropy present (Table 5). The Young's modulus was evaluated by the Oliver–Pharr method [31]. In addition to the measurements on the skutterudite specimens, a Young's modulus value of 82.0 ± 2.2 GPa was obtained for the 6061 aluminum standard specimen in this study (Table 5), which compares relatively well with the value of 85.5 ± 1.8 GPa found in a previous study using the same nanoindenter employed in this study [24] and the value of 85.0 ± 1.9 GPa obtained on a similar 6061 aluminum standard specimen nanoindented at Oak Ridge National Laboratory [24]. Thus, Young's modulus determined by nanoindentation in this study compares well with both Young's modulus values obtained previously on the same nanoindenter for the same aluminum alloy as well as the values obtained from another nanoindenter on the same aluminum alloy.

Comparing the RUS Young's modulus results (Table 3) with the nanoindentation results (Table 5), one finds that Young's moduli measured by nanoindentation is about 8% higher than the moduli measured by RUS. However, in the literature, it has been observed the values of Young's modulus determined by nanoindentation can exceed by several percent Young's modulus measured on the same specimens by nanoindentation. In a paper that directly compared the elastic modulus measurements obtained from four different techniques, namely Resonant Ultrasound Spectroscopy (RUS), impulse excitation, nanoindentation and the four-point bending test, Radovic et al. [32] found that nanoindentation measurements can be consistently higher than RUS measurements in some materials. For example, for aluminum metal, Young's modulus determined by nanoindentation measurements was about 10% higher than the moduli determined by RUS [32]. Also, Radovic et al. [32] found that for polycrystalline alumina with volume fraction porosities between roughly 0.01 and 0.04, the nanoindentation modulus was

Table 4
Literature values of Young's modulus, E, and shear modulus, G, and Poisson's ratio, ν, for n-type and p-type antimony-based skutterudites.

Composition	Type	Density (g/cm^3)	Relative density	E (GPa)	G (GPa)	ν	Ref.
Doped $CoSb_3$	n-Type	7.93–8.01	>0.99	137–141	60.7	0.14–0.25	[29]
$CoSb_3$	n-Type	7.55	0.991	148 ± 26	60 ± 13[a]	0.226 ± 0.048[a]	[30]
$CeFe_{3-x}Ru_xSb_4$[b]	p-Type	7.54–7.62	>0.99	133–139	53.8–54.3	0.22–0.29	[29]
$LaFe_4Sb_{12}$	p-Type	7.80	0.987	121 ± 20	57 ± 10[a]	0.235 ± 0.038[a]	[30]

[a] G and ν were not explicitly reported by Recknagel et al. [30]. The values of G and ν given here were calculated from Young's modulus and bulk modulus values given by Recknagel et al. [30].
[b] The dopant level indicated by "x" was not specified by Ravi et al. [29].

Table 5
Nanoindentation measurements of the mean and standard deviation of Young's modulus, E, and the assumed Poisson's ratio, ν[a], for multiple specimens cut from the indicated hot pressed billets, as well as an aluminum standard, Al6061. An assumed Poisson's ratio is required to calculate Young's modulus according to the Oliver–Pharr equation [31].

Billet label	Number of indentations	Type	Density (g/cm^3)	Relative density[a]	In pressing direction	E (GPa)	ν[a]
n-Ce-Wet1Side A	22	n-Type	7.59	0.977	No	154.7 ± 1.2	0.23
n-Ce-Wet1Side B	20	n-Type	7.59	0.977	No	153.1 ± 1.9	0.23
n-Ce-Wet1Side C	21	n-Type	7.59	0.977	Yes	149.8 ± 2.2	0.23
n-Wet2 Side A	18	n-Type	7.45	0.960	No	151.0 ± 2.6	0.23
n-Wet2 Side B	16	n-Type	7.45	0.960	No	147.5 ± 3.2	0.23
n-Wet2 Side C	20	n-Type	7.45	0.960	Yes	139.4 ± 2.5	0.23
Al 6061 Test 1	16	Metal	2.69	0.998	Not applicable	81.0 ± 2.1	0.33
Al 6061 Test 2	16	Metal	2.69	0.998	Not applicable	81.9 ± 1.8	0.33
Al 6061 Test 3	14	Metal	2.69	0.998	Not applicable	82.0 ± 2.0	0.33
Al 6061 Test 4	15	Metal	2.69	0.998	Not applicable	83.3 ± 2.4	0.33

[a] Density of SKD calculated was from lattice parameter reported by Recknagel et al. [30]. The measured density of 2.69 g/cm^3 for the aluminum standard compares well with the theoretical density of aluminum of 2.70 g/cm^3 [33].

higher than the modulus determined by RUS by roughly 7–10% [32].

4. Summary and conclusions

Powder processing and hot pressing of the (i) p-type ($Ce_{0.9}Fe_{3.5}Co_{0.5}Sb_{12}$) and (ii) n-type ($Co_{0.95}Pd_{0.05}Te_{0.05}Sb_3$ both with and without a 0.1 atomic% Ce addition skutterudite) yielded crack-free billets with relative mass densities ranging from approximately 96–98% of theoretical. Fracture surfaces of the hot pressed billets revealed mean grain sizes ranging from about 0.6 to 1.5 μm (Table 2). Pores roughly 1–3 μm across or smaller were present in both the n-type and p-type specimens, located predominantly along grain boundaries or at grain boundary triple points.

X-ray diffraction patterns for the Ce-doped and undoped specimens showed three broad peaks in the pattern for the Ce-doped specimen. The broad, low intensity peaks correspond to intense peaks in the $CoSb_2$ spectrum, but additional research needs to be done to determine whether, for example, $CoSb_2$ are present in the Ce-doped specimens and not in the undoped specimens.

For each of the four hot pressed skutterudite billets included in this study, the elastic moduli were quite uniform for specimens within each billet, as indicated by coefficient of variation values ranging from about 0.1 to 0.4% (Table 3). The mean elastic modulus of the Ce-doped n-type billet was very similar to the mean elastic moduli of the n-type billet without Ce-doping (Table 3). In addition to Young's modulus being uniform among the specimens cut from a given billet, nanoindentation measurements of three mutually orthogonal faces of a Ce-doped n-type specimen and an undoped n-type specimen indicate that these individual specimens showed no significant elastic anisotropy. The small (5% or less) differences between the elastic moduli of the pairs of p-type and n-type specimens may be due in part to the well-know effect of decreasing elastic moduli with increasing volume fraction porosity [28].

No elastic modulus data is available in the literature for the particular skutterudite compositions included in this study (Table 1). However, for other Sb-based skutterudite compositions, the literature values of elastic modulus are comparable to the elastic modulus values obtained in this study.

Acknowledgements

The authors acknowledge the financial assistance of the U.S. Department of Energy Grant DE-FC26-04NT42281. The authors also acknowledge the Defense University Research Instrumentation Program (DURIP) Grant No. N00014-09-1-0785, Office of Naval Research, which provided funding for the purchase of the Resonant Ultrasound Spectroscopy apparatus utilized in this research. The authors acknowledge the use of the nanoindentation equipment at the Composite Materials and Structures Center at Michigan State University. In addition, the authors thank Dr. Richard Staples, Department of Chemistry, Michigan State University his assistance with the XRD analysis.

References

[1] G. Kaiper, U.S. Energy Flow Trends – 2002, Office of Scientific and Technical Information, Oak Ridge, TN, 2004.
[2] D.M. Rowe, CRC Handbook on Thermoelectrics, CRC Press, Boca Raton, FL, 1995, p. 421.
[3] T.P. Hogan, A. Downey, J. Short, J. D'Angelo, C.-I. Wu, E. Quarez, J. Androulakis, P.F.P. Poudeu, J.R. Sootsman, D.-Y. Chung, M.G. Kanatzidis, S.D. Mahanti, E.J. Timm, H. Schock, F. Ren, J. Johnson, E.D. Case, Nanostructured thermoelectric materials and high efficiency power generation modules, J. Electron. Mater. 36 (2007) 704–710.
[4] J. Yang, T. Caillat, Thermoelectric materials for space and automotive power generation, Mater. Res. Bull. 31 (2006) 224–229.
[5] F. Stabler, Automotive Applications of High Efficiency Thermoelectrics, Presented at DARPA/ONR Program Review and DOE High Efficiency Thermoelectric Workshop San Diego, CA, March 24–27, 2002.
[6] T. Caillat, J.P. Fleurial, A. Borschevsky, Preparation and thermoelectric properties of semiconducting Zn_4Sb_3, J. Phys. Chem. Solids 58 (1997) 1119–1125.
[7] C. Uher, J. Yang, S. Hu, D.T. Morelli, G.P. Meisner, Transport properties of pure and doped MNiSn (M = Zr, Hf), Phys. Rev. B 59 (1999) 8615–8621.
[8] G.S. Nolas, M. Kaeser, R. Littleton IV, T.M. Tritt, High figure of merit in partially filled ytterbium skutterudite materials, Appl. Phys. Lett. 77 (2000) 1855–1857.
[9] V.N. Kaliakin, Introduction to Approximate Solution Techniques, Numerical Modeling, and Finite Element Methods, Marcel Dekker, Inc., New York, 2002.
[10] J.N. Reddy, An Introduction to the Finite Element Method, 3rd edition, McGraw-Hill Higher Education, New York, 2006.
[11] E.D. Case, The saturation of thermomechanical fatigue in brittle materials, in: M.H. Alibadi (Ed.), Thermo-mechanical Fatigue and Fracture, WIT Press, Southampton, UK, 2002, pp. 137–208.
[12] E.D. Case, Y. Kim, The effect of surface-limited microcracks on the effective Young's modulus of ceramics, J. Mater. Sci. 28 (1993) 1885–1900.
[13] E.D. Case, C. Glinka, Characterization of microcracks in $YCrO_3$ using small angle neutron scattering and elasticity measurements, J. Mater. Sci. 19 (1984) 2962–2968.
[14] F. Ren, E.D. Case, A. Morrison, M. Tafesse, M.J. Baumann, Young's modulus, shear modulus and Poisson's ratio as a function of porosity for alumina and hydroxyapaptite, Philos. Mag. 89 (2009) 1163–1182.
[15] J.E. Ni, F. Ren, E.D. Case, E.J. Timm, Porosity dependence of elastic moduli in LAST (lead–antimony–silver–tellurium) thermoelectric materials, Mater. Chem. Phys. 118 (2009) 459–466.
[16] J. Jiang, L.D. Chen, S.Q. Bai, Q. Yao, Q. Wang, Thermoelectric properties of textured p-type $(Bi,Sb)_2Te_3$ fabricated by spark plasma sintering, Scripta Mater. 52 (2005) 347–351.
[17] J. Jiang, L.D. Chen, S.Q. Bai, Q. Yao, Q. Wang, Fabrication and thermoelectric performance of textured n-type $Bi_2(Te,Se)_3$ by spark plasma sintering, Mater. Sci. Eng. B: Solid 117 (2005) 334–338.
[18] F. Ren, E.D. Case, E.J. Timm, M.D. Jacobs, H.J. Schock, Weibull analysis of the biaxial fracture strength of a cast p-type LAST-T thermoelectric material, Philos. Mag. Lett. 86 (2006) 673–682.
[19] S.S. Kim, S. Yamamoto, T. Aizawa, Thermoelectric properties of anisotropy-controlled p-type Bi–Te–Sb system via bulk mechanical alloying and shear extrusion, J. Alloys Compd. 375 (2004) 107–113.
[20] A.L. Pilchak, F. Ren, E.D. Case, E.J. Timm, H.J. Schock, C.-I. Wu, T.P. Hogan, Characterization of dry milled powders of LAST (lead–antimony–silver–tellurium) thermoelectric material, Philos. Mag. 87 (2007) 4567–4591.

[21] B.D. Hall, E.D. Case, F. Ren, J.R. Johnson, E.J. Timm, Agglomeration during wet milling of LAST (lead–antimony–silver–tellurium) powders, Mater. Chem. Phys. 113 (2009) 497–502.
[22] A. Migliori, J.L. Sarrao, Resonant Ultrasound Spectroscopy: Applications to Physics, Materials Measurements, and Nondestructive Evaluation, Academic Press, New York, 1997.
[23] F. Ren, E.D. Case, J.R. Sootsman, M.G. Kanatzidis, H. Kong, C. Uher, E. Lara-Curzio, R.M. Trejo, C. Uher, The high temperature elastic moduli of polycrystalline PbTe measured by resonant ultrasound spectroscopy, Acta Mater. 56 (2008) 5954–5963.
[24] F. Ren, E.D. Case, J.E. Ni, E.J. Timm, E. Lara-Curzio, R.M. Trejo, C.-H. Lin, M.G. Kanatzidis, Temperature-dependent elastic moduli of lead telluride-based thermoelectric materials, Philos. Mag. 89 (2009) 143–167.
[25] W.F. McClure (Ed.), Powder Diffraction File Sets 19 to 20, International Centre for Diffraction Data, Swarthmore, PA, 1979, p. 107.
[26] W.F. McClure (Ed.), Powder Diffraction File Sets 29 to 30, International Centre for Diffraction Data, Swarthmore, PA, 1987, p. 50.
[27] B.D. Cullity, S.R. Stock, Elements of X-ray Diffraction, 3rd ed., Prentice Hall, Upper Saddle River, NJ, 2001, Chapter 5.
[28] R.W. Rice, Mechanical Properties of Ceramics and Composites, Marcel Dekker, New York, 2000, pp. 308–312.
[29] V. Ravi, S. Firdosy, T. Caillat, B. Lerch, A. Calamino, R. Pawlik, M. Nathal, A. Sechrist, J. Buchhalter, S. Nutt, Mechanical properties of thermoelectric skutterudites, in: Mohamed S. El-Genk (Ed.), Proceedings of Space Technology and Applications International Forum – STAIF 2008, vol. 969, American Institute of Physics Conference Proceedings, Albuquerque, NM, 10–14 February 2008, 2008, pp. 656–662.
[30] C. Recknagel, N. Reinfried, P. Höhn, W. Schnelle, H. Rosner, Yu. Grin, A. Leithe-Jasper, Application of spark plasma sintering to the fabrication of binary and ternary skutterudites, Sci. Technol. Adv. Mater. 8 (2007) 357–363.
[31] W.C. Oliver, G.M. Pharr, An improved technique for determining hardness and elastic modulus using load and displacement sensing indentation experiments, J. Mater. Res. 7 (1992) 1564–1583.
[32] M. Radovic, E. Lara-Curzio, L. Reister, Comparison of different experimental techniques for determination of elastic properties of solids, Mater. Sci. Eng. A 368 (2004) 56–70.
[33] Aluminum Association, International Alloy Designations and Chemical Composition Limits for Wrought Aluminum and Wrought Aluminum Alloys, Arlington, VA, 2009.